Eur. Phys. J. B **58**, 379–387 (2007)
DOI: 10.1140/epjb/e2007-00249-5

THE EUROPEAN PHYSICAL JOURNAL B

Acoustic phonon transmission spectra in piezoelectric AlN/GaN Fibonacci phononic crystals

P.D. Sesion Jr[1], E.L. Albuquerque[1,a], C. Chesman[1], and V.N. Freire[2]

[1] Departamento de Física, Universidade Federal do Rio Grande do Norte, 59072-970 Natal-RN, Brazil
[2] Departamento de Física, Universidade Federal do Ceará, Campus do Pici 60455-760 Fortaleza-CE, Brazil

Received 2 May 2007 / Received in final form 14 August 2007
Published online 22 September 2007 –

Abstract. We study the acoustic-phonon transmission spectra in periodic and quasiperiodic (Fibonacci type) superlattices made up from the III-V nitride materials AlN and GaN. The phonon dynamics is described by a coupled elastic and electromagnetic equations within the static field approximation model, stressing the importance of the piezoelectric polarization field in a strained condition. We use a transfer-matrix treatment to simplify the algebra, which would be otherwise quite complicated, allowing a neat analytical expressions for the phonon transmission coefficients. Numerical results, for the normal incidence case, show a strike self-similar pattern for both hexagonal (class 6 mm) and cubic symmetries crystalizations of the nitrides.

PACS. 63.20.Dj Phonon states and bands, normal modes, and phonon dispersion – 63.22.+m Phonons or vibrational states in low-dimensional structures and nanoscale materials – 77.65.-j Piezoelectricity and electromechanical effects

1 Introduction

The study of phononic crystals, which are periodic composite materials with lattice spacings comparable to the acoustic wavelength, has received increasing attention during the last decade driven by acoustoelectronic devices in modern communication systems (for an up to date review see [1]). They ultimately offer control of the propagation of acoustic or elastic waves on a wavelength scale, being the acoustic analogues of photonic crystals for the case of optical and electromagnetic waves. They consist of two- or three-dimensional periodic arrangements of two materials with differing elastic constants that can give rise to absolute acoustic stop bands under well-chosen geometrical conditions.

These composite materials can exhibit several interesting acoustic phonons physical properties, such as their possible role in sound filters, transducer design and acoustic mirrors, to cite just a few [2]. Besides, layered composites may support novel types of waves, with specific frequency dependence not found in homogeneous substrates, an old subject of solid state physics [3].

It is clear, on general grounds, that in a specimen consisting of alternate layers of thickness d_a of material A and thickness d_b of material B, the periodicity produces a Brillouin zone boundary at reciprocal wavevector $Q = \pi/(d_a + d_b)$. One effect of this zone boundary is that the acoustic phonon dispersion curve becomes folded to a zig-zag within the first Brillouin zone, yielding frequency gaps (i.e. stop bands) in the phonon dispersion relation, thus allowing a phonon-filtering action in the stop bands. As typical values of the layers thicknesses are 20 nm, the Brillouin zone edge at $Q/2\pi = [2(d_a + d_b)]^{-1}$ occurs at around 10^5 cm^{-1}, meaning that a significant fraction of the Brillouin zone is accessible to inelastic light scattering techniques. Indeed, it was recently proposed hypersonic phononic crystals to control the emission and propagation of high frequency phonons by using interference lithography, whose direct measurement of their phononic band structure is possible via Brillouin light scattering [4].

Phononic devices based on piezoelectric materials are attractive since they are extensively used as radio-frequency filters in wireless telecommunication systems: the integration of a phononic band gap structure to such devices would enhance their characteristics and widen their application range. From a fundamental point of view, piezoelectric phononic crystals enable experiments in which the sources and detectors of acoustic waves can be embedded with the phononic crystal itself [5]. The strong anisotropy of acoustic wave propagation inherent to piezoelectric materials, combined with the mixing of shear and longitudinal polarizations, strongly affect wave scattering, opening up further prospects for designing a generation of phononic-crystal-based acoustic signal processing devices.

[a] e-mail: eudenilson@dfte.ufrn.br

On the other hand, quasiperiodic crystals are a unique type of structures which lack long-range translational symmetry but possess a certain orientation order. An appealing motivation for studying such structures is that their structural order lie at the boundary between the translational invariant crystals and the random glass materials. Besides, they exhibit a highly fragmented energy spectrum displaying a self-similar pattern. Indeed, from a strictly mathematical perspective, it has been proven that their spectra are Cantor sets in the thermodynamic limit (for an up to date review see [6]). Recently, polaritonic states in piezoelectric Fibonacci and Thue-Morse quasiperiodic structures were investigated, considering the dynamics of the electromagnetic and the acoustic waves treated on equal footing [7].

It is our aim in this work to investigate the acoustic-phonon transmission spectra in multilayer structures composed of III-V nitride semiconductors AlN/GaN, layers arranged in a periodic and quasiperiodic Fibonacci type fashion. The III-V nitride materials, such as GaN and AlN, display important piezoelectric polarization fields in a strained condition and is of obvious importance for the study of nitride-based piezodevices and multilayer structures [8]. In particular, knowledge of these properties allows an insightful treatment of the polarization and ensuing electric fields in strained and polarized nitride junctions and superlattices under any strain condition. They can crystallize in both hexagonal wurtzite or cubic zinc-blend structures [9]. The wurtzite crystals have a different unit cell structure (four atoms per unit cell with nine optical and three acoustic phonons for a given wavevector), as well as a lower symmetry when compared to the cubic zinc-blende counterpart, leading to a different carrier-phonon interaction.

Although significant advances in growth, doping, and device application of group III-V nitride materials have been achieved with their stable wurtzite hexagonal phase [10], less progress has been made with their metastable zinc-blend cubic structure. However, devices with a zinc-blend structure would have considerable advantages. This is particularly true for GaN due to its higher saturated electron drift velocity, easy cleavage, and lower band energy [11,12]. Also cubic nitrides are expected to have higher mobility, due to the decrease of the phonon number for the higher symmetry structure. Therefore, information on the vibrational properties of both structures (hexagonal and cubic) are strongly desirable.

The hexagonal wurtzite structures are uniaxial crystals with the optical axis coinciding with the Cartesian z-axis, which is perpendicular to the hexagons (forming the xy-plane). It is the structure with highest symmetry compatible and its polarization, as its cubic counterpart, has a strain-induced piezoelectric field $\delta\vec{P}$, given by [13]

$$\delta P_i = e_{ijk} s_{jk}, \tag{1}$$

which should be considered besides the spontaneous polarization in the equilibrium structure. Here repeated subscript are summed over, and ijk can be any Cartesian x, y, or z axis. Also, e_{ijk} is the third rank piezoelectric tensor, and s_{kl}, the strain tensor, is defined by:

$$s_{jk} = (1/2)\left(\frac{\partial u_j}{\partial r_k} + \frac{\partial u_k}{\partial r_j}\right), \tag{2}$$

u_k being the displacement along the coordinate axes r_k.

The presence of this piezoelectric polarization component prevents us to use the much simpler continuum equation

$$\rho \partial^2 u_i/\partial t^2 = \partial S_{ij}/\partial r_j \tag{3}$$

to describe the acoustic phonon dynamics (see next section). In equation (3), ρ is the density of the material (GaN and AlN), and S_{ij} is the stress tensor, given by $S_{ij} = C_{ijkl} s_{kl}$, where C_{ijkl} is the 4th-order elastic tensor. We consider also a transfer-matrix treatment to simplify the algebra, which would be otherwise quite complicated, that allows one to obtain a neat analytical expressions for the phonon transmission coefficients. Previous works in this subject have considered the elastic band structure [14] and the electromechanical coupling coefficient of a surface acoustic wave [15] in a two-dimensional phononic crystal containing piezoelectric material. The Lyapunov exponents in ordered and disordered piezoelectric phononic crystals [16] as well as their acoustic phonon's localization, scale law and the parametric spectrum of singularities $f(\alpha)$, were recently presented and discussed [17].

The plan of this work is as follows: we start in Section 2 with our theoretical model along with some physical parameters definitions. The transfer-matrix approach used as a mathematical tool to determine the acoustic-phonon spectra is presented in Section 3. Further, in Section 4, the phonon transmission spectra is shown, with their main features discussed, with special emphasis in the striking self-similar pattern for normal incidence. Section 5 deals with some concluding remarks.

2 Acoustic phonon dynamics

We now present our general theory to study the vibration modes in piezoelectric materials. The piezoelectric term responsible for the coupled elastic and electromagnetic fields is usually weak enough to allow the hybrid wave solution to behave like a quasielastic mode, with a phase velocity slightly lower than the uncoupled elastic mode, and a quasielectromagnetic mode, with a phase velocity shifted to a slightly higher value than the electromagnetic wave. As the electromagnetic wave has a velocity approximately five orders of magnitude higher than the elastic wave, we can describe the former in the static field approximation in which the particle displacement u_j $(j = x, y, z)$ along the coordinate axes r_j is coupled, through the piezoelectric tensor e_{ijk}, to the electrical potential ϕ by the following set of equations [18]:

$$\rho \frac{\partial^2 u_j}{\partial t^2} - C_{ijkl} \frac{\partial^2 u_k}{\partial r_i \partial r_l} - e_{kij} \frac{\partial^2 \phi}{\partial r_i \partial r_k} = 0, \tag{4}$$

$$e_{ikl} \frac{\partial^2 u_k}{\partial r_i \partial r_l} - \varepsilon_{ik} \frac{\partial^2 \phi}{\partial r_i \partial r_k} = 0, \tag{5}$$

where i, j, k and l can be x, y, or z with repeated subscript summed over. Also, ε_{ik} is the second rank dielectric permittivity tensor defined by:

$$\varepsilon(\omega) = \begin{pmatrix} \varepsilon_{xx}(\omega) & 0 & 0 \\ 0 & \varepsilon_{xx}(\omega) & 0 \\ 0 & 0 & \varepsilon_{zz}(\omega) \end{pmatrix}. \quad (6)$$

Here ε_{xx} and ε_{zz} are the dielectric functions perpendicular and parallel to the z-axis, respectively. They are given by (neglecting any damping effect):

$$\varepsilon_{xx} = \varepsilon_\infty \frac{\omega^2 - \omega_{LO,E_1}^2}{\omega^2 - \omega_{TO,E_1}^2}, \quad (7)$$

$$\varepsilon_{zz} = \varepsilon_\infty \frac{\omega^2 - \omega_{LO,A_1}^2}{\omega^2 - \omega_{TO,A_1}^2}, \quad (8)$$

where ε_∞ is the high-frequency dielectric constant, and $\omega_{TO,X}$ ($\omega_{LO,X}$) is the transverse optical (longitudinal optical) phonon angular frequency for the mode X, for each crystalline structure (cubic and hexagonal). Here X means either the irreducible representation of $A_1(z)$ (z-axis) or $E_1(xy)$ (xy-plane) at the Γ point.

Assuming that the hybrid wave is propagating in the x-direction with a phase velocity equal to ω/q_x, the solutions of equations (4) and (5) can be cast into the forms:

$$u_j = \alpha_j \exp(ikz) \exp(iq_x x - i\omega t), \quad j = x, y, z, \quad (9)$$

$$\phi = \alpha_4 \exp(ikz) \exp(iq_x x - i\omega t), \quad (10)$$

where the $\alpha' s$ coefficients are the amplitudes of the different components. Substitution of the solutions of equations (9) and (10) into the coupled equations (4) and (5) yields coupled differential equations for the pairs (u_x, u_z) and (u_y, ϕ) for both symmetries (hexagonal and cubic), where in the latter the coupling is due to the piezoelectric tensor. For the wurtzite (hexagonal) structure, taking into account the appropriate form of the elastic and piezoelectric tensor [19], and considering only the piezoelectric case of interest to us, i.e. the pair (u_y, ϕ), these equations are reduced to:

$$-\rho\omega^2 u_y - C_{44}\left(\frac{\partial^2 u_y}{\partial z^2} + \frac{\partial^2 u_y}{\partial x^2}\right) - e_{x5}\left(\frac{\partial^2 \phi}{\partial z^2} + \frac{\partial^2 \phi}{\partial x^2}\right) = 0, \quad (11)$$

$$e_{x5}\left(\frac{\partial^2 u_y}{\partial z^2} + \frac{\partial^2 u_y}{\partial x^2}\right) - \varepsilon_{xx}\frac{\partial^2 \phi}{\partial x^2} + \varepsilon_{zz}\frac{\partial^2 \phi}{\partial z^2} = 0, \quad (12)$$

where C_{44} and e_{x5} are the components of the elastic and piezoelectric tensors, respectively (from now on we will use the short notation C_{IJ} and e_{iJ} for simplicity). Solving these coupled equations we obtain (omitting the common $\exp(iq_x x)$ factor):

$$u_y = B_1 \exp(ik_1 z) + B_2 \exp(-ik_1 z) - (e_{x5}/C_{44}) L(k_2)\Big[B_3 \exp(ik_2 z) + B_4 \exp(-ik_2 z)\Big], \quad (13)$$

$$\phi = (e_{x5}/\varepsilon_{zz}) L(k_1)\Big[B_1 \exp(ik_1 z) + B_2 \exp(-ik_1 z)\Big] + B_3 \exp(ik_2 z) + B_4 \exp(-ik_2 z). \quad (14)$$

Here B_r ($r = 1, 2, 3, 4$) are unknowns coefficients to be determined through the boundary conditions, and $k_{1,2} = (k_\pm)^{1/2}$, where

$$k_\pm^2 = \frac{(q_{Tz}^2 - k_x^2 - 2q_x^2 p \pm \Delta)}{2(1+p)}. \quad (15)$$

Also,

$$\Delta = \Big[(q_{Tz}^2 + k_x^2)^2 + 4p(q_{Tz}^2 + q_x^2)(k_x^2 - q_x^2)\Big]^{1/2}, \quad (16)$$

$$q_{Tz}^2 = (\omega/v_T)^2 - q_x^2, \quad (17)$$

$$k_x^2 = (\varepsilon_{xx}/\varepsilon_{zz}) q_x^2, \quad (18)$$

$$L(k_1) = (k_1^2 + q_x^2)/(k_1^2 + k_x^2), \quad (19)$$

$$L(k_2) = (k_2^2 + q_x^2)/(k_2^2 - q_{Tz}^2). \quad (20)$$

In the above equations, $p = (e_{x5}^2/\varepsilon_{zz} C_{44})$, q_{Tz} (q_x) is the z- (x-) component of the transverse wavevector of the elastic wave, whose transverse velocity v_T is given by $v_T = (C_{44}/\rho)^{1/2}$. Observe that when the piezoelectric coupling is zero ($p = 0$), equation (15) yields the limits $k_+^2 = q_{Tz}^2$ and $k_-^2 = -k_x^2$, as it should be.

On the other hand, for the zinc-blend (cubic) symmetry one finds:

$$-\rho\omega^2 u_y - C_{44}\left(\frac{\partial^2 u_y}{\partial z^2} + \frac{\partial^2 u_y}{\partial x^2}\right) - 2e_{x4}\frac{\partial^2 \phi}{\partial x \partial z} = 0, \quad (21)$$

$$2e_{x4}\frac{\partial^2 u_y}{\partial x \partial z} - \varepsilon_{xx}\frac{\partial^2 \phi}{\partial x^2} + \varepsilon_{zz}\frac{\partial^2 \phi}{\partial z^2} = 0, \quad (22)$$

whose solutions are:

$$u_y = L(k_1')\Big[B_1' \exp(ik_1' z) - B_2' \exp(-ik_1' z)\Big] + (\varepsilon_{xx}/e_{x4}) L(k_2')\Big[B_3' \exp(ik_2' z) - B_4' \exp(-ik_2' z)\Big], \quad (23)$$

$$\phi = (e_{x4}/\varepsilon_{xx})\Big[B_1' \exp(ik_1' z) + B_2' \exp(-ik_1' z)\Big] + B_3' \exp(ik_2' z) + B_4' \exp(-ik_2' z). \quad (24)$$

Here $k_{1,2}' = (k_\pm')^{1/2}$, with $k_\pm'$ given by

$$k_\pm' = [(q_{Tz}^2 - k_x^2 - 4q_x^2 p') \pm \Delta']/2. \quad (25)$$

Also,

$$\Delta' = \Big[(q_{Tz}^2 + k_x^2)^2 + 8q_x^2 p'(k_x^2 + 2q_x^2 p' - q_{Tz}^2)\Big]^{1/2}, \quad (26)$$

$$L(k') = \Big[k'^3 + k' q_x^2 [(\varepsilon_{xx}/\varepsilon_{zz}) + 4p']\Big] \Big/ 2q_x q_{Tz}^2, \quad (27)$$

and $p' = e_{x4}^2/\varepsilon_{zz} C_{44}$.

In the next section we will use the expressions found for the elastic displacement u_y and the electrical potential ϕ to determine the phonons's transmission coefficients using a suitable transfer-matrix approach.

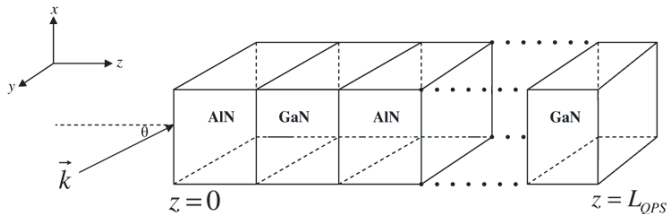

Fig. 1. The schematic representation showing the geometry of the quasiperiodic multilayer system considered in this work, as a sequence of alternating stacking of AlN and GaN constituents layers following a Fibonacci arrangement.

3 Transfer matrix approach

Now we turn to the simplest case considered here, namely the periodic binary superlattice composed of zinc-blende (cubic) and wurtzite (hexagonal) GaN/AlN layers, forming a binary superlattice structure, namely, $\cdots$/ AlN/GaN / $\cdots$ /substrate, where the substrate is here considered to be a transparent dielectric medium like vacuum (see Fig. 1). The more complex quasiperiodic Fibonacci structure will be considered later, as a generalization of the situation treated here. We will consider first both nitride layers with a hexagonal wurtzite crystalline structure, whose unit cell has thickness $L_{PS} = d_a + d_b$, where d_a (d_b) is the thickness of the AlN (GaN) layer.

For the superlattice bulk modes, the coupled field equations, defined by equations (11) and (12), together with the elastic and electromagnetic boundary conditions at the nth unit cell, i.e., the interfaces $z = nL_{PS} + d_a$ (AlN/GaN) and $z = (n+1)L_{PS}$ (GaN /AlN), yield:

(a) by imposing continuity of the transverse displacement u_y:

$$A_1^n f_{a1} + A_2^n \bar{f}_{a1} - \lambda_{1a} L(k_{2a}) A_3^n f_{a2} - \lambda_{1a} L(k_{2a}) A_4^n \bar{f}_{a2} = B_1^n + B_2^n - \lambda_{1b} L(k_{2b}) B_3^n - \lambda_{1b} L(k_{2b}) B_4^n, \quad (28)$$

$$A_1^{n+1} + A_2^{n+1} - \lambda_{1a} L(k_{2a}) A_3^{n+1} - \lambda_{1a} L(k_{2a}) A_4^{n+1} = B_1^n f_{b1} + B_2^n \bar{f}_{b1} - \lambda_{1b} L(k_{2b}) B_3^n f_{b2} - \lambda_{1b} L(k_{2b}) B_4^n \bar{f}_{b2}. \quad (29)$$

(b) by imposing continuity of the electrical potential ϕ:

$$\lambda_{2a} L(k_{1a}) A_1^n f_{a1} + \lambda_{2a} L(k_{1a}) A_2^n \bar{f}_{a1} + A_3^n f_{a2} + A_4^n \bar{f}_{a2} = \lambda_{2b} L(k_{1b}) B_1^n + \lambda_{2b} L(k_{1b}) B_2^n + B_3^n + B_4^n, \quad (30)$$

$$\lambda_{2a} L(k_{1a}) A_1^{n+1} + \lambda_{2a} L(k_{1a}) A_2^{n+1} + A_3^{n+1} + A_4^{n+1} = \lambda_{2b} L(k_{1b}) B_1^n f_{b1} + \lambda_{2b} L(k_{1b}) B_2^n \bar{f}_{b1} + B_3^n f_{b2} + B_4^n \bar{f}_{b2}. \quad (31)$$

(c) by imposing continuity of the transverse stress tensor S_{32}:

$$\mu k_{1a}[1 + p_a L(k_{1a})]\Big[A_1^n f_{a1} - A_2^n \bar{f}_{a1}\Big] + \mu\lambda_{1a} k_{2a}[1 - L(k_{2a})]\Big[A_3^n f_{a2} - A_4^n \bar{f}_{a2}\Big] = k_{1b}[1 + p_b L(k_{1b})]\Big[B_1^n - B_2^n\Big] + \lambda_{1b} k_{2b}[1 - L(k_{2b})]\Big[B_3^n - B_4^n\Big], \quad (32)$$

$$\mu k_{1a}[[1 + p_a L(k_{1a})]\Big[A_1^{n+1} - A_2^{n+1}\Big] + \mu\lambda_{1a} k_{2a}[1 - L(k_{2a})]\Big[A_3^{n+1} - A_4^{n+1}\Big] = k_{1b}[1 + p_b L(k_{1b})]\Big[B_1^n f_{b1} - B_2^n \bar{f}_{b1}\Big] + \lambda_{1b} k_{2b}[1 - L(k_{2b})]\Big[B_3^n f_{b2} - B_4^n \bar{f}_{b2}\Big]. \quad (33)$$

(d) by imposing continuity of the normal component of the electrical displacement D_z:

$$\lambda_{2a}(k_{1a}/k_{2b})[L(k_{1a}) - 1]\Big[A_1^n f_{a1} - A_2^n \bar{f}_{a1}\Big] + (k_{2a}/k_{2b})[p_a L(k_{2a}) + 1]\Big[A_3^n f_{a2} - A_4^n \bar{f}_{a2}\Big] = \lambda_{2b}(\varepsilon_{zzb}/\varepsilon_{zza})(k_{1b}/k_{2b})[L(k_{1b}) - 1]\Big[B_1^n - B_2^n\Big] + (\varepsilon_{zzb}/\varepsilon_{zza})[p_b L(k_{2b}) + 1]\Big[B_3^n - B_4^n\Big], \quad (34)$$

$$\lambda_{2a}(k_{1a}/k_{2b})[L(k_{1a}) - 1]\Big[A_1^{n+1} - A_2^{n+1}\Big] + (k_{2a}/k_{2b})[p_a L(k_{2a}) + 1]\Big[A_3^{n+1} - A_4^{n+1}\Big] = \lambda_{2b}(\varepsilon_{zzb}/\varepsilon_{zza})(k_{1b}/k_{2b})[L(k_{1b}) - 1]\Big[B_1^n f_{b1} - B_2^n \bar{f}_{b1}\Big] + (\varepsilon_{zzb}/\varepsilon_{zza})[p_b L(k_{2b}) + 1]\Big[B_3^n f_{b2} - B_4^n \bar{f}_{b2}\Big]. \quad (35)$$

In the above equations we have used the following definitions ($m = a, b$; $j = 1, 2$):

$$f_{mj} = \exp(ik_{jm} d_m) = 1/\bar{f}_{mj}, \quad (36)$$

$$\lambda_{1m} = e_{x4m}/C_{44m}; \;\; \lambda_{2m} = e_{x5m}/\varepsilon_{zzm}, \quad (37)$$

$$\mu = C_{44a}/C_{44b}. \quad (38)$$

Defining the kets formed by the unknowns coefficients

$$|A^{(n)}\rangle = \begin{pmatrix} A_1^{(n)} \\ A_2^{(n)} \\ A_3^{(n)} \\ A_4^{(n)} \end{pmatrix}, \quad (39)$$

with similar expression for $|B^{(n)}\rangle$, equations (28) to (35) can be expressed as the matrices equations:

$$M_1 |A^{(n)}\rangle = N_1 |B^{(n)}\rangle, \quad (40)$$

$$M_2 |A^{(n+1)}\rangle = N_2 |B^{(n)}\rangle, \quad (41)$$

$$M_1 = \begin{pmatrix} f_{a1} & \bar{f}_{a1} & -\lambda_{1a}L(k_{2a})f_{a2} & -\lambda_{1a}L(k_{2a})\bar{f}_{a2} \\ \mu k_{1a}[1+p_aL(k_{1a})]f_{a1} & -\mu k_{1a}[1+p_aL(k_{1a})]\bar{f}_{a1} & \mu\lambda_{1a}k_{2a}[1-L(k_{2a})]f_{a2} & -\mu\lambda_{1a}k_{2a}[1-L(k_{2a})]\bar{f}_{a2} \\ \lambda_{2a}L(k_{1a})f_{a1} & \lambda_{2a}L(k_{1a})\bar{f}_{a1} & f_{a2} & \bar{f}_{a2} \\ \lambda_{2a}\frac{k_{1a}}{k_{2b}}[L(k_{1a})-1]f_{a1} & -\lambda_{2a}\frac{k_{1a}}{k_{2b}}[L(k_{1a})-1]\bar{f}_{a1} & \frac{k_{2a}}{k_{2b}}[1+p_aL(k_{2a})]f_{a2} & -\frac{k_{2a}}{k_{2b}}[1+p_aL(k_{2a})]\bar{f}_{a2} \end{pmatrix}, \quad (42)$$

$$N_1 = \begin{pmatrix} 1 & 1 & -\lambda_{1b}L(k_{2b}) & -\lambda_{1b}L(k_{2b}) \\ k_{1b}[1+p_bL(k_{1b})] & -k_{1b}[1+p_bL(k_{1b})] & \lambda_{1b}k_{2b}[1-L(k_{2b})] & -\lambda_{1b}k_{2b}[1-L(k_{2b})] \\ \lambda_{2b}L(k_{1b}) & \lambda_{2b}L(k_{1b}) & 1 & 1 \\ \lambda_{2b}\frac{\varepsilon_{zzb}}{\varepsilon_{zza}}\frac{k_{1b}}{k_{2b}}[L(k_{1b})-1] & -\lambda_{2b}\frac{\varepsilon_{zzb}}{\varepsilon_{zza}}\frac{k_{1b}}{k_{2b}}[L(k_{1b})-1] & \frac{\varepsilon_{zzb}}{\varepsilon_{zza}}[1+p_aL(k_{2b})] & -\frac{\varepsilon_{zzb}}{\varepsilon_{zza}}[1+p_bL(k_{2b})] \end{pmatrix}. \quad (43)$$

$$M_1' = \begin{pmatrix} L(k'_{1a})f'_{a1} & -L(k'_{1a})\bar{f}'_{a1} & \frac{L(k'_{2a})}{\lambda'_{2a}}f'_{a2} & -\frac{L(k'_{2a})}{\lambda'_{2a}}\bar{f}'_{a2} \\ \mu[L(k'_{1a})k'_{1a}+q_xp'_a]f'_{a1} & \mu[L(k'_{1a})k'_{1a}+q_xp'_a]\bar{f}'_{a1} & \mu[\frac{k'_{2a}}{\lambda'_{2a}}L(k'_{1a})+q_xp'_a]f'_{a2} & \mu[\frac{k'_{2a}}{\lambda'_{2a}}L(k'_{1a})+q_xp'_a]\bar{f}'_{a2} \\ \lambda'_{2a}f'_{a1} & \lambda'_{2a}\bar{f}'_{a1} & f'_{a2} & \bar{f}'_{a2} \\ \lambda'_{2a}k'_{1a}f'_{a1} & -\lambda'_{2a}k'_{1a}\bar{f}'_{a1} & k'_{2a}f'_{a2} & -k'_{2a}\bar{f}'_{a2} \end{pmatrix}, \quad (44)$$

$$N_1' = \begin{pmatrix} L(k'_{1b}) & -L(k'_{1b}) & \frac{L(k'_{2b})}{\lambda'_{2b}} & -\frac{L(k'_{2b})}{\lambda'_{2b}} \\ L(k'_{1b})k'_{1b}+q_xp'_b & L(k'_{1b})k'_{1b}+q_xp'_b & \frac{k'_{2b}}{\lambda'_{2b}}L(k'_{1b})+q_xp'_b & \frac{k'_{2b}}{\lambda'_{2b}}L(k'_{1b})+q_xp'_b \\ \lambda'_{2b} & \lambda'_{2b} & 1 & 1 \\ \frac{\varepsilon_{zzb}}{\varepsilon_{zza}}\lambda'_{2b}k'_{1b} & -\frac{\varepsilon_{zzb}}{\varepsilon_{zza}}\lambda'_{2b}k'_{1b} & \frac{\varepsilon_{zzb}}{\varepsilon_{zza}}k'_{2b} & -\frac{\varepsilon_{zzb}}{\varepsilon_{zza}}k'_{2b} \end{pmatrix}. \quad (45)$$

where

see equation (42) above

and

see equation (43) above

The matrix M_2 is obtained from M_1 by dividing the first row by f_{a1}, the second by $\bar{f}_{a1}$, the third by f_{a2}, and the fourth by $\bar{f}_{a2}$. Similarly, we can obtain the matrix N_2 from N1 by multiplying the first row by f_{b1}, the second by $\bar{f}_{b1}$, the third by f_{b2}, and the fourth by $\bar{f}_{b2}$.

In a similar way we can carry out the case cubic zinc-blend crystalline structure. The results are similar to those found for the cubic case, with M_1' given by

see equation (44) above

and

see equation (45) above

Furthermore, the matrix M_2' can be found in the same way as discussed in the cubic case. The matrix N_2' can be obtained from the matrix N_1' by multiplying the first row by f'_{b1}, the second by $\bar{f}'_{b1}$, the third by f'_{b2}, and the fourth by $\bar{f}'_{b2}$. Besides, p'_m $(m = 1, 2)$ is defined as for p_m, provided we replace e_{x5m} by e_{x4m}.

It is easy to show that, using equations (40) and (41) one can find:

$$|A^{(n+1)}\rangle = T|A^{(n)}\rangle, \quad (46)$$

where in the last step Blochs ansatz was used. Here T, the so-called transfer matrix, is given by:

$$T = M_2^{-1}N_2N_1^{-1}M_1. \quad (47)$$

We now turn our attention to the quasiperiodic structures. In order to construct them, we define briefly here the rules of the unit cell growth, that consists of a sequence of building blocks (or layers), where the arrangement of the layers follows the desired sequence. For the well-known Fibonacci (FB) sequence, the rule is $S_n = S_{n-1}S_{n-2}$, $n > 2$, where $S_1 = A$, $S_2 = AB$. The FB rule is invariant under the transformation $A \to AB$ and $B \to A$. Here A means the AlN layer, while B represents the GaN one. These inflation rules can also be understood as an invariance condition, because they leave their respective sequences invariant when applied. The Fibonacci generations are:

$$S_0 = [B];\ S_1 = [A];\ S_2 = [AB];\ S_3 = [ABA];\ \text{etc.} \quad (48)$$

The number of the bulding blocks increases according to the Fibonacci number, $F_l = F_{l-1} + F_{l-2}$ (with $F_0 = F_1 = 1$), and the ratio between the number of the building blocks A and the number of the building blocks B in the sequence is equal to the golden mean number $\tau = (1/2)(1+\sqrt{5})$.

To determine the phonon transmission curves for the quasiperiodic FB structure we can use the appropriated transfer matrices, which for the wurtzite hexagonal structure for any higher generation ($n \geq 1$) is given by $T_{S_{n+2}} = T_{S_n}T_{S_{n+1}}$, with a similar expression for the cubic zinc-blend structure (provided we replace all hexagonal M's and N's matrices by their cubic counterparts). Therefore, from the knowledge of the transfer matrices $T_{S_0} = N_2^{-1}M_2$, $T_{S_1} = N_1^{-1}M_1$, and $T_{S_2} = N_1^{-1}M_2N_2^{-1}M_1$ (periodic case), we can determine the transfer matrix of any FB generation.

4 Phonon transmission spectra

As explained in the previous section, for piezoelectric materials with hexagonal (class 6 mm) and cubic symmetries, equations (9) and (10) yield coupled differential equations for the pairs (u_x, u_z) (shear vertical waves) and (u_y, ϕ) (shear horizontal waves), respectively, where in the latter the coupling is due to the piezoelectric tensor. Under these circumstances, in order to obtain the transmission spectra we must relate the amplitudes of the elastic field in the

transparent medium (vacuum) C at $z < 0$ to those in the region $z > L_{QPS}$, L_{QPS} being the size of the quasiperiodic structure, by successive applications of equation (46) which relates the amplitudes A_i^{n+1} of the elastic field in layer $(n+1)$ with those A_i^n associated to the layer n.

To do that, let us consider the transmission geometry depicted in Figure 1, where the phonon wavevector $\vec{k}$ makes an incident angle θ to the growth direction of the quasiperiodic structure (z-axis).

Re-arranging equation (46) to take into account the boundary conditions at the interfaces $z < 0$ and $z > L_{QPS}$ [20], we obtain:

$$\begin{pmatrix} A_1^n \\ A_2^n \\ A_3^n \\ A_4^{n+1} \end{pmatrix} = D^{-1} D' \begin{pmatrix} A_1^{n+1} \\ A_2^{n+1} \\ A_3^{n+1} \\ A_4^n \end{pmatrix}, \tag{49}$$

where

$$D = \begin{pmatrix} T_{11} & T_{12} & T_{13} & 0 \\ T_{21} & T_{22} & T_{23} & 0 \\ T_{31} & T_{32} & T_{33} & 0 \\ T_{41} & T_{42} & T_{43} & -1 \end{pmatrix}, \tag{50}$$

and

$$D' = \begin{pmatrix} 1 & 0 & 0 & -T_{14} \\ 0 & 1 & 0 & -T_{24} \\ 0 & 0 & 1 & -T_{34} \\ 0 & 0 & 0 & -T_{44} \end{pmatrix}. \tag{51}$$

Once equation (49) is solved, the transmittance can be obtained by:

$$T = \frac{\mid A_1^{n+1} \mid^2}{\mid A_1^n \mid^2}. \tag{52}$$

Now we present numerical simulations for the acoustic phonon transmission through the quasiperiodic AlN/GaN piezoelectric multilayered structure. The physical parameters used here are:

(i) for AlN [21]: $\omega_{LO,E_1} = 113.02$, $\omega_{TO,E_1} = 83.13$, $\varepsilon_\infty = 4.68$, $\rho = 3.32$, $C_{44} = 2.00$, $e_{x4} = 1.46$ and $e_{x5} = 0.60$;
(ii) for GaN [22]: $\omega_{LO,E_1} = 94.06$, $\omega_{TO,E_1} = 73.22$, $\varepsilon_\infty = 5.29$, $\rho = 6.25$, $C_{44} = 1.54$, $e_{x4} = 0.73$ and $e_{x5} = 0.49$.

Here, the frequencies are in units of meV, the elastic terms in units of 10^{11} N/m^2, the piezoelectric terms in units of C/m^2, and the densities in units of 10^3 kg/m^3. We have considered the thickness of the AlN layer d_a equal to 10 nm, and the ratio $d_a/d_b = 0.5$. For numerical results, instead of to use the frequency ω, we prefer to replace it by the reduced frequency ω/Ω, with $\Omega = v_T/d_a$.

The normal incidence ($\theta = 0$) acoustic phonon transmission spectrum for the tenth-generation (89 layers) quasiperiodic Fibonacci sequence, as a function of the reduced dimensionless frequency ω/Ω, is shown in Figure 2a, for the hexagonal symmetry. The transmission spectrum presents a filtering action on phonons around the reduced frequency $\omega/\Omega = 2.375$, corresponding to a forbidden gap (stop band). Besides, the structure is phonon transparent (the transmission coefficient is closely equal to 1.0)

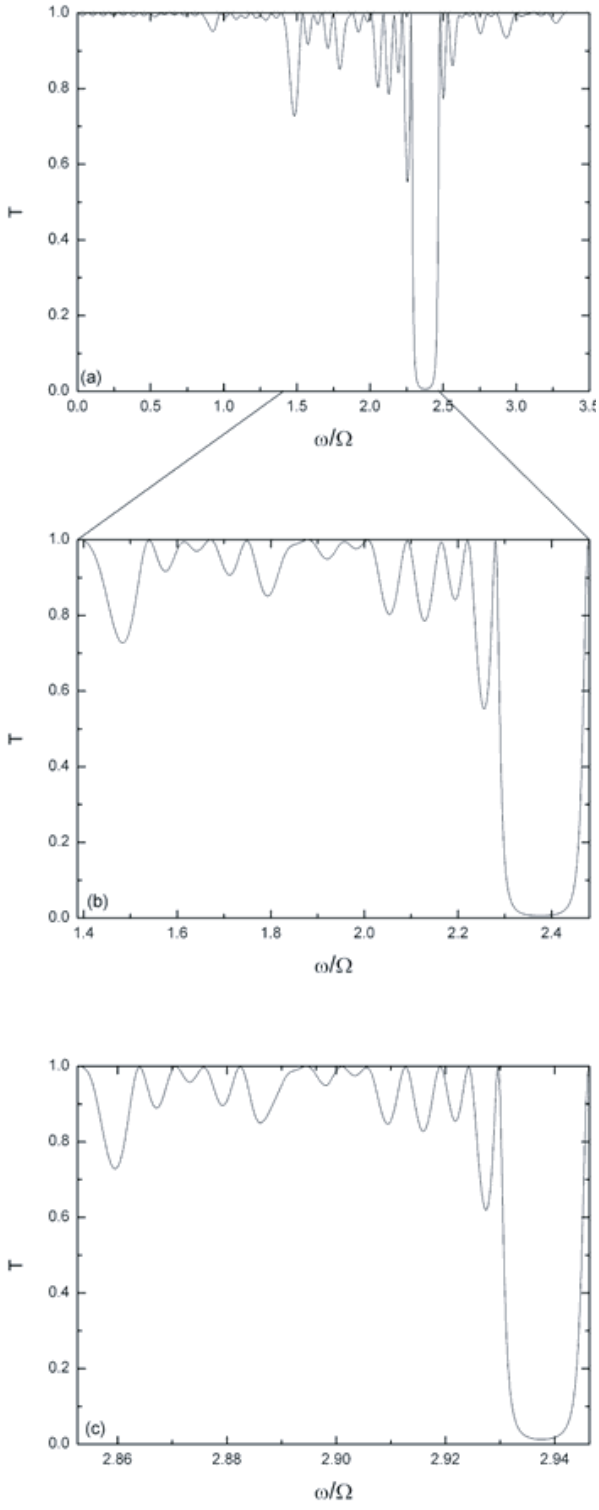

Fig. 2. Normal-incidence acoustic phonon transmission spectra for the quasiperiodic Fibonacci multilayered phononic structure in the hexagonal symmetry: (a) the transmittance T as a function of the reduced frequency ω/Ω, with $\Omega = v_T/d_a$, for the tenth generation of the Fibonacci sequence; (b) same as in (a), but for the reduced range of frequency $1.38 < \omega/\Omega < 2.48$; (c) same as in (b), but for the fifteenth generation of the Fibonacci sequence, at the range of frequency $2.852 < \omega/\Omega < 2.946$.

at several reduced frequencies. The condition of transparentness implies that the layers A (AlN) and B (GaN) are equivalent from a wave point of view. Furthermore, the transmission spectrum has a striking scaling property with respect to the generation number of the Fibonacci sequence. To understand this scaling property, consider Figure 2b, which shows the optical transmission spectrum of Figure 2a for the range $1.38 < \omega/\Omega < 2.48$. This spectrum is the same, as shown in Figure 2c, to the one representing the fifteenth-generation (987 layers) quasiperiodic Fibonacci sequence (i.e. it has been recovered after five Fibonacci generation), for the range of frequency reduced by a scale factor f approximately equal to 10 ($2.852 < \omega/\Omega < 2.946$). So, f gives the scale change of the acoustic wavevector between spectra $T[S_j]$ and $T[S_{j+5}]$, S_j being the jth generation of the Fibonacci sequence. Indeed, at the twentieth-generation, which means 10,946 layers (not shown here), this striking self-similar pattern appears again for the range of frequency ($2.979 < \omega/\Omega < 2.988$), which is reduced by a scale factor equal to f^2 (approximately 100). Therefore, quasilocalization of the acoustic waves in a Fibonacci phononic multilayer is demonstrated by the self-similarity of the transmission coefficients under the given boundary conditions.

Analogously, the normal incidence acoustic phonon transmission spectrum for the tenth-generation Fibonacci sequence, as a function of the reduced dimensionless frequency ω/Ω, is shown in Figure 3a, for the cubic symmetry. The filtering action on the acoustic phonons appears now in a two much broad range of frequency, the first one at $1.249 < \omega/\Omega < 1.40$, with the other at $2.585 < \omega/\Omega < 2.710$, defining two stop bands. As in the hexagonal symmetry case, the transmission spectrum is phonon transparent at several reduced frequencies, with the same striking scaling property with respect to the generation number of the Fibonacci sequence, as it can be seen in Figure 3b, which shows the optical transmission spectrum of Figure 3a for the range of frequency $1.10 < \omega/\Omega < 1.46$. As it is depicted in Figure 3c, this spectrum is recovered again after five Fibonacci generation, i.e. at the fifteenth-generation, for the range of frequency reduced by a scale factor approximately equal to 10 ($1.622 < \omega/\Omega < 1.660$), and again at the twentieth-generation (not shown here), at the frequency range defined by ($0.9137 < \omega/\Omega < 0.9164$).

For the oblique case, Figure 4 shows quite a different scenery for the hexagonal symmetry. The transmission spectrum shows now a sharp stop band for the incident angle $\theta = 10°$ (full line) at $\omega/\Omega = 1.652$. This sharp forbidden band develops into a broad band, as the angle of incidence increases, reaching the frequency range $1.5 < \omega/\Omega < 1.65$ for the incident angle $\theta = 45°$ (dashed line). Observe a new sharp forbidden band at the low-frequency region, at $\omega/\Omega = 0.409$. Quite interesting, there is no more self-similar structure, indicating that the phonon transmission is very sensitive to the angle of incidence. On the other hand, for the cubic symmetry, the transmission spectra shows, as in the normal incidence case, two stop bands at different frequencies range, for different incident angles. For the the low-frequency regions (depicted in Fig. 5) the sharp dips are at $\omega/\Omega = 0.572$ for the incident angle $\theta = 45°$ (dashed line), and $\omega/\Omega = 1.648$ for $\theta = 10°$ (full line).

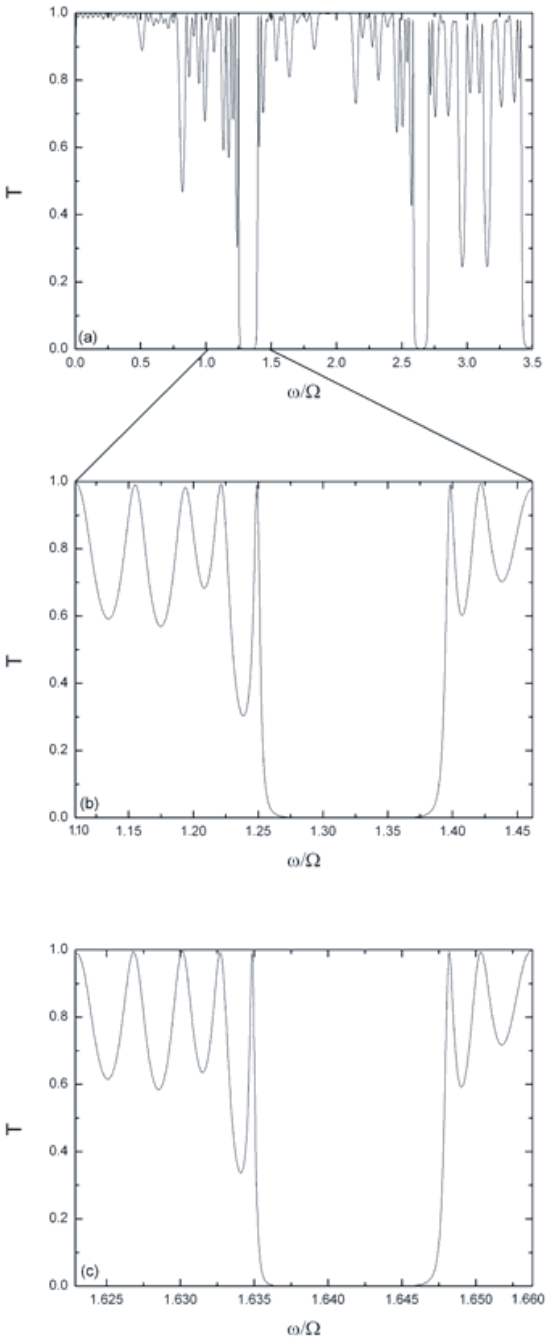

Fig. 3. Normal-incidence acoustic phonon transmission spectra for the quasiperiodic Fibonacci multilayered phononic structure in a cubic symmetry: (a) the transmittance T as a function of the reduced frequency ω/Ω, with $\Omega = v_T/d_a$, for the tenth generation of the Fibonacci sequence; (b) same as in (a), but for the reduced range of frequency $1.10 < \omega/\Omega < 1.46$; (c) same as in (b), but for the fifteenth generation of the Fibonacci sequence, at the range of frequency $1.622 < \omega/\Omega < 1.660$.

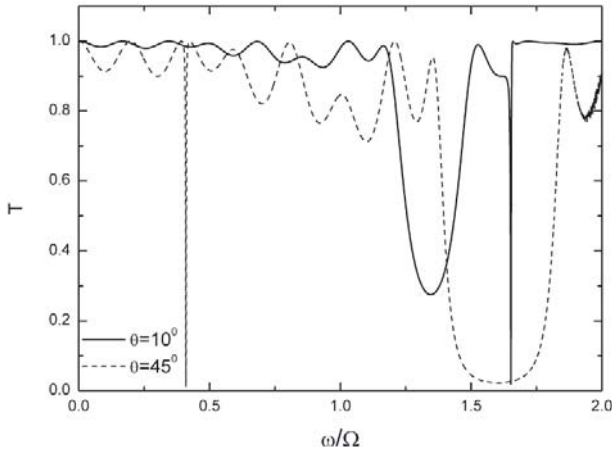

Fig. 4. Oblique-incidence acoustic phonon transmission spectra for the seventh generation Fibonacci phononic structure in the hexagonal symmetry: (a) $\theta = 10°$ (full line); (b) $\theta = 45°$ (dotted line).

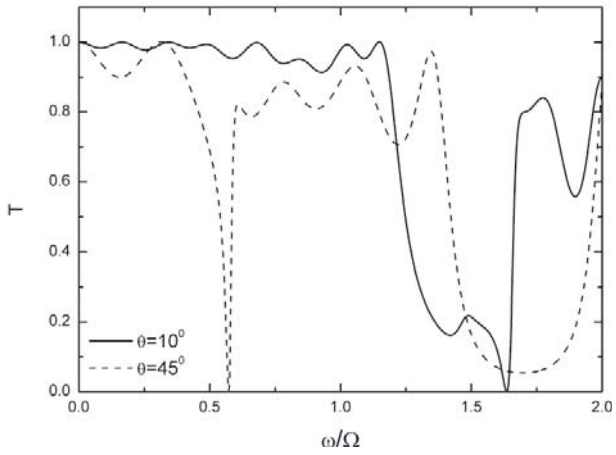

Fig. 5. Same as in Figure 4, but for the cubic symmetry.

For a better insight of the transmission spectra dependence on the incident angle, we have shown in Figure 6 the angular dependence of the phonon transmission spectra for the seventh generation Fibonacci phononic structure as a function of $\sin^2(\theta)$, for a fixed value of the dimensionless reduced frequency $\omega/\Omega = 1.0$, considering both symmetries: the hexagonal symmetry (full line), and the cubic one (dotted line). This angular dependence of the phonon transmission at a fixed frequency provides complementary information on the resonant characteristics of phonons in the quasiperiodic multilayer system. The hexagonal symmetry (full line) presents a smooth profile for the transmission spectra, with dips (forbidden bands) at $\omega/\Omega = 0.335$ and 0.980. Comparing with the hexagonal symmetry case, the cubic one (dotted line) presents several sharp enhancements in transmission in the dip regions, indicating the existence of resonances. Both symmetries are very sensitive to the choice of the incident angle, with interesting different transmission behaviors. The strong dependence of the phonon transmission spectra on the angle of incidence is due to the presence of the intermode Bragg

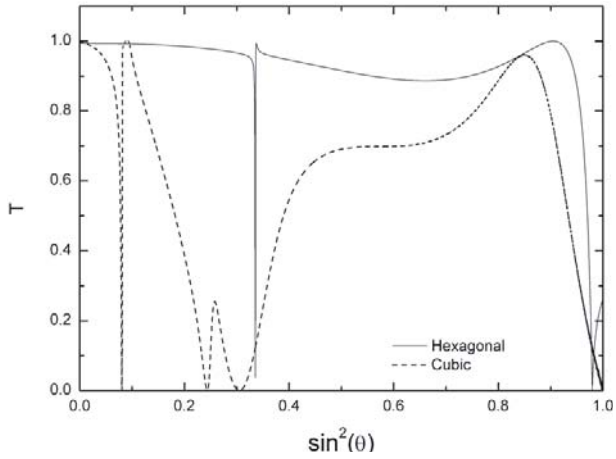

Fig. 6. The transmission spectra for the seventh generation Fibonacci phononic structure, as a function of $\sin^2(\theta)$, for a fixed value of the dimensionless reduced frequency $\omega/\Omega = 1.0$: hexagonal symmetry (full line); cubic symmetry (dotted line).

reflection, in addition to the ordinary intramode Bragg reflection presented also in the normal incidence case [23]. Besides, the intermode Bragg reflection yields a frequency gap of the spectrum inside the folded Brillouin zone of the multilayer structure, breaking the self-similar pattern presented in the normal incidence case. Furthermore, the opacity (or transparency) of the multilayer structure can be monitored using appropriated angle of incidence, and we believe that the information found here could help experimental works on this subject.

5 Concluding remarks

In summary, we have described the transmission spectra for acoustic phonons propagating in periodic and quasiperiodic (Fibonacci type) semiconductor phononic crystals using a theoretical model beyond the elastic continuum approach. We have considered stacking of wurtzite (hexagonal) and zinc blende (cubic) semiconductor structures of GaN and AlN. These promising results open additional prospects for phononic devices exploiting phononic band-gap properties suggesting, for instance, the potential of designing the phonon filtering action by combining generations of the Fibonacci quasiperiodic structures. Quite surprisingly we found that the phononic band-gap are indeed very sensitive to the choice of the incident angle, with interesting different transmission behaviors. The opacity (or transparency) of the structure can be monitored using appropriated angle of incidence, and we believe that the information described here is encouraging for possible experimental works on this subject.

The most important experimental technique used to probe these phonon modes is the Brillouin light scattering, and indeed it was previously been successfully applied for high-quality free-standing GaN substrate [24] as well as GaN thin film on sapphire substrate [25].

We would like to thank partial financial support from the Brazilian Research Agency CNPq-Rede Nanobioestruturas.

References

1. M. Sigalas, M.S. Kushwaha, E.N. Economou, M. Kafesaki, I.E. Psarobas, W. Steurer, Z. Krist. **220**, 765 (2005)
2. A. Khelif, A. Choujaa, B. Djafari-Rouhani, M. Wilm, S. Ballandras, V. Laude, Phys. Rev. B **68**, 0214301 (2003); A. Khelif, A. Choujaa, S. Benchabane, B. Djafari-Rouhani, V. Laude, Appl. Phys. Lett. **84**, 4400 (2004); Y. Pennec, B. Djafari-Rouhani, J.O. Vasseur, A. Khelif, P.A. Deymier, Phys. Rev. E **69**, 046608 (2004)
3. E.L. Albuquerque, R. Loudon, D.R. Tilley, J. Phys. C: Solid State Phys. **12**, 5297 (1979); E.L. Albuquerque, R. Loudon, D.R. Tilley, J. Phys. C: Solid State Phys. **13**, 1775 (1980); E.L. Albuquerque, J. Phys. C: Solid State Phys. **13**, 2623 (1980)
4. T. Gorishnyy, C.K. Ullal, M. Maldovan, G. Fytas, E.L. Thomas, Phys. Rev. Lett. **94**, 115501 (2005)
5. S. Benchabane, A. Khelif, J.-Y. Rauch, L. Robert, V. Laude, Phys. Rev. E **73**, 065601(R) (2006)
6. E.L. Albuquerque, M.G. Cottam, Phys. Rep. **376**, 225 (2003); E.L. Albuquerque, M.G. Cottam, *Polaritons in Periodic and Quasiperiodic Structures* (Elsevier, Amsterdam, 2004)
7. Z. Liu, W. Zhang, Phys. Rev. B **72**, 134304 (2005); Z. Liu, W. Zhang, Phys. Rev. B **75**, 064207 (2007)
8. A. Bykhovski, B. Gelmont, M. Shur, A. Khan, J. Appl. Phys. **77**, 1616 (1995)
9. B. Gil, *Group III Nitride Semiconductor Compounds* (Clarendon, Oxford, 1998)
10. F. Bernardini, V. Fiorentini, D. Vanderbilt, Phys. Rev. B **56**, R10024 (1997)
11. G. Ramirez-Flores, H. Navarro-Contreras, A.L Astras-Martinez, Phys. Rev. B **50**, 8433 (1994)
12. K.H. Ploog, O. Brandt, H. Yang, T. Trampert, Thin Solid Films **306**, 231 (1997)
13. J. Gleize, J. Frandon, M.A. Renucci, F. Bechstedt, Phys. Rev. B **63**, 073308 (2001)
14. Z.L Hou, F.G. Wu, Y. Liu, Solid State Commun. **130**, 745 (2004)
15. T.T. Wu, Z.C Hsu, Z.G. Huang, Phys. Rev. B **71**, 064303 (2005)
16. F.M. Li, M.Q. Xu, Y.S. Wang, Solid State Commun. **141**, 296 (2007)
17. P.D. Sesion Jr, E.L. Albuquerque, M.S. Vasconcelos, P.W. Mauriz, V.N. Freire, Eur. Phys. J. B **51**, 583 (2006)
18. B.A. Auld, *Acoustic Fields and Waves in Solids* (R.E. Krieger Publish Company, Malabar, Fl, 1990), Vols. 1 and 2
19. J.F. Nye, *Physical Properties of Crystals* (Clarendon, Oxford, 1985)
20. G. Monsivais, J.A. Otero, H. Calás, Phys. Rev. B **71**, 064101 (2005)
21. P. Perlin, A. Polian, T. Suski, Phys. Rev. B **47**, 2874 (1993)
22. F. Bechstedt, U. Grossner, J. Furthmller, Phys. Rev. B **62**, 8003 (2000)
23. S. Tamura, Phys. Rev. B **43**, 12646 (1991)
24. M. Yamaguchi, T. Yagi, T. Sota, T. Deguchi, K. Shimada, S. Nakamura, J. Appl. Phys. **85**, 8502 (1999)
25. M. Yamaguchi, T. Yagi, T. Azuhata, T. Sota, K. Suzuki, S. Chichibu, S. Nakamura, J. Phys.: Condens. Matter **9**, 241 (1997)